NR1D1 Stimulates Antitumor Immune Responses in Breast Cancer by Activating cGAS-STING Signaling

Na-Lee Ka[1,2], Mi Kyung Park[3], Seung-Su Kim[1], Yoon Jeon[4], Sewon Hwang[1], Sun Mi Kim[3], Ga Young Lim[1], Ho Lee[3], and Mi-Ock Lee[1,2,5]

ABSTRACT

Potentiating antitumor immunity is a promising therapeutic approach for treating a variety of cancers, including breast cancer. One potential strategy to promote antitumor immunity is targeting DNA damage response. Given that the nuclear receptor NR1D1 (also known as REV-ERBα) inhibits DNA repair in breast cancer cells, we explored the role of NR1D1 in antitumor $CD8^+$ T-cell responses. First, deletion of *Nr1d1* in MMTV-PyMT transgenic mice resulted in increased tumor growth and lung metastasis. Orthotopic allograft experiments suggested that loss of *Nr1d1* in tumor cells rather than in stromal cells played a prominent role in increasing tumor progression. Comprehensive transcriptome analyses revealed that biological processes including type I IFN signaling and T cell–mediated immune responses were associated with NR1D1. Indeed, the expression of type I IFNs and infiltration of $CD8^+$ T cells and natural killer cells in tumors were suppressed in *Nr1d1*$^{-/-}$;MMTV-PyMT mice. Mechanistically, NR1D1 promoted DNA damage–induced accumulation of cytosolic DNA fragments and activated cGAS-STING signaling, which increased the production of type I IFNs and downstream chemokines CCL5 and CXCL10. Pharmacologic activation of NR1D1 by its ligand, SR9009, enhanced type I IFN–mediated antitumor immunity accompanied by the suppression of tumor progression and lung metastasis. Taken together, these findings reveal the critical role of NR1D1 in enhancing antitumor $CD8^+$ T-cell responses, suggesting that NR1D1 may be a good therapeutic target for breast cancer.

Significance: NR1D1 suppresses breast cancer progression and lung metastasis by enhancing antitumor immunity via cGAS-STING pathway activation, which provides potential immunotherapeutic strategies for breast cancer.

Introduction

Breast cancer is the most frequently diagnosed cancer and the leading cause of cancer-related deaths in women worldwide (1). Breast cancer is a heterogeneous disease composed of distinct subtypes with different biological and morphologic features, and disparate responses to treatment (2). Despite great improvements in diagnosis and therapeutics, 20%–30% of patients with breast cancer may develop metastases and the 5-year overall survival rate of patients with distant metastasis is less than 20% (3). There are still limited treatment options for patients with metastatic breast cancer; thus, it is critical to identify novel therapeutic targets for the development of effective strategies against metastatic breast cancer.

In the tumor microenvironment (TME), the immune system functions as a double-edged sword in cancer, as it can protect against tumor development by eliminating neoplastic cells but promotes tumor immune escape by shaping tumor immunogenicity (4). Thus, it is of great significance to reestablish the host antitumor immune response to successfully eradicate cancer. Although breast cancer has been historically considered a poorly immunogenic tumor, it was recently reported that certain breast cancer cases have a high tumor mutational burden and are strongly infiltrated by immune cells (5). A number of clinical studies have shown that the presence of tumor-infiltrating lymphocytes (TIL) at diagnosis confers both prognostic and predictive value, especially in triple-negative breast cancer (TNBC) and $HER2^+$ breast cancer (6–8). High levels of TILs are also associated with improved prognosis in metastatic breast cancer (9, 10). The extent and function of TILs are modulated by multiple factors including type I IFNs. Produced by tumor cells and infiltrating immune cells, type I IFNs promote the maturation and activation of antigen-presenting cells to facilitate T-cell cross-priming and infiltration into tumors (11). Thus, many attempts have been made to induce type I IFN responses to reshape the TME and enhance immunogenicity (11).

The stimulator of IFN genes (STING) pathway is critical for inducing type I IFNs to elicit antitumor immunity. Sensing of cytosolic DNA by cyclic guanosine monophosphate–adenosine monophosphate synthase (cGAS) leads to the activation of STING and downstream signaling molecules, including TANK-binding kinase 1 (TBK1) and IFN regulatory factor 3 (IRF3). In turn, these lead to the increased expression of type I IFNs and downstream chemokines, such as CC chemokine ligand 5 (CCL5) and C-X-C motif chemokine ligand 10 (CXCL10), which induce the infiltration and activation of cytotoxic T cells and natural killer (NK) cells to the tumor sites (12). DNA damage and the resulting leakage of genomic DNA are sources of cytoplasmic DNA, which can trigger the STING pathway and subsequent immune response in cancer cells (13). Defects in DNA repair factors such as ataxia-telangiectasia mutated (*ATM*), breast cancer

[1]College of Pharmacy, Seoul National University, Seoul, Republic of Korea. [2]Research Institute of Pharmaceutical Sciences, Seoul National University, Seoul, Republic of Korea. [3]Graduate School of Cancer Science and Policy, National Cancer Center, Gyeonggi, Republic of Korea. [4]Research Institute, National Cancer Center, Gyeonggi, Republic of Korea. [5]Bio-MAX institute, Seoul National University, Seoul, Republic of Korea.

N.-L. Ka and M.K Park contributed equally to this article

Corresponding Authors: Mi-Ock Lee, College of Pharmacy, Seoul National University, 1 Gwanak-ro, Gwanak-gu, Seoul 08826, Republic of Korea. Phone: 822-880-9331; Fax: 822-887-2692; E-mail: molee@snu.ac.kr; and Ho Lee, Graduate School of Cancer Science and Policy, National Cancer Center, 323 Ilsan-ro, Ilsandong-gu, Goyang-si Gyeonggi-do 10408, Republic of Korea. Phone: 823-1920-2274; E-mail: ho25lee@ncc.re.kr

Cancer Res 2023;83:3045–58

doi: 10.1158/0008-5472.CAN-23-0329

gene 1/2 (*BRCA 1/2*), bloom syndrome protein, excision repair cross complementing-group 1, and ribonuclease H2 subunit A, cause high levels of cytosolic DNA, which trigger STING signaling and cell-intrinsic type I IFN responses (13). Breast tumors with a DNA damage response (DDR)-deficient signature, those recognizing loss of the Fanconi anemia/*BRCA* DNA repair pathway, show STING activation and $CD8^+$ T-cell infiltration (14). We also showed that defect in the repair of DNA double-strand breaks (DSB) caused by the IFN γ-inducible protein 16-type I IFN axis enhances STING-mediated type I IFN signaling and antitumor immune responses in TNBC (15). Thus, DDR regulators could be good candidates to modulate the antitumor immune response.

Nuclear receptor subfamily 1 group D member 1 (NR1D1), also known as REV-ERBα, is a circadian clock component that integrates circadian rhythm and metabolism (16). NR1D1 has been implicated in a variety of pathophysiologic processes including inflammation, metabolic diseases, and cancer (17). The *NR1D1* gene is coamplified with *ERBB2* at the 17q12–q21 chromosomal region in breast tumors, which is associated with poor clinical outcomes (18, 19). NR1D1 has also been shown to promote the proliferation of ERBB2 (HER2)-positive breast cancer cells (20). However, recent studies have shown that NR1D1 harbors tumor-suppressive functions. *NR1D1* transcript levels are significantly lower in a number of breast cancer cells compared with noncancer mammary epithelial cells (21). Activation of NR1D1 with a synthetic agonist, SR9011, suppresses the proliferation of breast cancer cells by directly targeting cyclin A2 expression and arresting the cell cycle (22). Furthermore, activation of NR1D1 by SR9009 exerts cytotoxic effects on a variety of cancer cells, including breast cancer, without affecting normal cells, by suppressing *de novo* lipogenesis and autophagy, which are essential cellular processes for the survival of tumor cells (23). Importantly, we previously reported that NR1D1 inhibits DNA repair in breast cancer cells through binding on DSB sites, where it suppresses further recruitment of DDR factors (24). Considering the importance of the DDR in antitumor immune responses, we investigated the role of NR1D1 and its ligands in breast cancer in the context of antitumor immunity.

Materials and Methods

Analyses of breast cancer patient cohort and human breast cancer tissue microarray

Expression levels of *NR1D1* in breast cancer and adjacent normal tissues obtained from The Cancer Genome Atlas (TCGA) RNA-sequencing (RNA-seq) database were analyzed using the Breast Cancer Integrative Platform (BCIP; http://www.omicsnet.org/bcancer/; ref. 25). The GSE37751 dataset was downloaded from NCBI Gene Expression Omnibus (GEO; http://www.ncbi.nlm.nih.gov/geo/; ref. 26). Kaplan–Meier plotter mRNA breast cancer database (http://kmplot.com/analysis/) was utilized to assess the prognostic value of NR1D1 in breast cancer (probe ID 31637_s_at or 204760_s_at; ref. 27). The processed data including normalization procedures were obtained from the corresponding websites, and no additional transformations were performed.

Human breast tissue microarray slides (BN08111, BR1191, and BR247a) that contains breast carcinoma tissues, normal adjacent breast tissues, and normal breast tissues were purchased from TissueArray.Com LLC. The slides were subjected to immunostaining with anti-NR1D1 antibody (Supplementary Table S1). Imaging and quantification was performed using the Vectra Polaris Automated Quantitative Pathology Imaging System and inForm software (Akoya Biosciences).

Animal studies

Nr1d1 knockout (KO) mouse in FVB/N (RRID: MGI:6112021) or in C57BL/6J (RRID: IMSR_JAX:000664) were generated using the CRISPR/Cas9 system (ToolGen, Inc.); mixture of 100 ng/μL Cas9 protein (M0646T, New England Biolabs) and 50 ng/μL gRNA was injected to the cytoplasm of pronuclei (Supplementary Table S2). Indel mutations in F1 mice were identified by sequencing. All mice were genotyped at 4 weeks after birth and housed according to their gender (Supplementary Table S2). FVB/N-*Nr1d1*$^{+/-}$ mice were crossbred with mouse mammary tumor virus–polyoma middle tumor-antigen (MMTV-PyMT; designated as PyMT) mice (RRID: IMSR_JAX:002374). At 14 weeks of age, mice were sacrificed and mammary tumors and lung were removed and fixed in formalin, and paraffin-embedded for further analyses. To visualize system-wide tumor burden, *Nr1d1*$^{+/-}$; PyMT mice were crossbred with MMTV-FP635 (designated as FP635) mice (kindly provided by Prof. Jiyoung Park in UNIST, Ulsan, South Korea), in which fluorescence is exclusively expressed in the mammary ductal epithelium under the control of MMTV promoter (28). Tumor progression in *Nr1d1*;FP635;PyMT mice was monitored using the IVIS 200 imaging system (Xenogen Corporation) and signal intensity was analyzed with Living image software (version 4.5.5; PerkinElmer).

For the orthotopic xenograft, control-Py230 or *Nr1d1* KO-Py230 cells (established as described below) resuspended in Matrigel (BD Biosciences) were injected into the mammary fat pads of C57BL/6J-*Nr1d1*$^{+/+}$ [designated as *Nr1d1* wild-type (WT)] or *Nr1d1*$^{-/-}$ (*Nr1d1* KO) mice. Eight weeks after the injection of tumor cells, mice were sacrificed and primary tumor and lungs were removed. To examine the effects of SR9009 on tumor growth in MMTV-PyMT model, mice were administrated with vehicle or 100 mg/kg SR9009 for 5 times a week for 6 weeks by intraperitoneal injection. All mice were sacrificed at 10 am considering that *Nr1d1* is a circadian clock gene. The animal studies were reviewed and approved by the Institutional Animal Care and Use Committee (IACUC) of the National Cancer Center Research Institute (NCCRI; protocols: NCC-20–545, NCC-21–714, and NCC-21–678), which is an Association for Assessment and Accreditation of Laboratory Animal Care International accredited facility that abides by the Institute of Laboratory Animal Resources guide. All animal experiments were performed in accordance with the guidelines for the Care and Use of Laboratory Animals of the IACUC of the National Cancer Center Research Institute.

Cell culture and reagents

Human breast cancer cell lines MDA-MB-231 (RRID: CVCL_0062), SKBR3 (RRID: CVCL_0033), MCF7 (RRID: CVCL_0031), T47D (RRID: CVCL_0553), BT474 (RRID: CVCL_0553), BT549 (RRID: CVCL_1092), and Hs578T (RRID: CVCL_0332), a murine breast cancer cell line, Py230 (RRID: CVCL_AQ08), and a human nontumorigenic breast epithelial cell line, MCF10A (RRID: CVCL_0598), were obtained from the ATCC. MDA-MB-231, MCF7, BT474, and Hs578T cells were maintained in DMEM supplemented with 10% FBS. SKBR3, T47D, and BT549 cells were maintained in RPMI1640 medium supplemented with 10% FBS. Py230 cells were maintained in Ham F-12K (Kaighn's) medium supplemented with 5% FBS. MCF10A cells were maintained in DMEM-F12 (1:1) medium supplemented with 5% FBS, 20 ng/mL EGF, 0.5 μg/mL hydrocortisone, and 10 μg/mL insulin. To generate *NR1D1* KO sublines, cells were transfected with an *NR1D1* CRISPR/Cas9 KO plasmid (sc-401211 or sc-432177, Santa Cruz Biotechnology) or a control plasmid (sc-418922) using Lipofectamine 2000 (Thermo Fisher Scientific). GFP-positive cells were sorted by FACS Aria (BD Biosciences), and *NR1D1* KO was confirmed by Western blotting after expansion of clones. The cells were grown in an incubator with 5%

CO_2/95% air at 37°C. Cells were authenticated using short tandem repeat analysis and routinely certified free of *Mycoplasma* contamination using the MycoAlert Mycoplasma Detection Kit (Lonza). H_2O_2, doxorubicin, cisplatin, and GSK4112 were purchased from Sigma-Aldrich. SR9009 were purchased from APExBIO.

Transcriptomic analyses

For RNA-seq analysis, total RNA was obtained from the mammary gland tumor tissues of 14-week-old FVB/N-*Nr1d1* WT;PyMT and *Nr1d1* KO;PyMT mice. mRNA enrichment and library preparation were performed using the NEBNext Ultra II Directional RNA-Seq Kit (New England Biolabs) following the manufacturer's protocol. mRNA was isolated using the Poly(A) RNA Selection Kit (LEXOGEN, Inc.) and used for the cDNA synthesis and shearing. Indexing was performed using the Illumina indexes 1–12. After enrichment step was carried out using PCR, the libraries were evaluated using the TapeStation HS D1000 Screen Tape (Agilent Technologies) for the mean fragment size. Quantification was performed using the library quantification kit using a StepOne Real-Time PCR System (Life Technologies, Inc.). High-throughput sequencing was performed as paired-end 100 sequencing using NovaSeq 6000 (Illumina, Inc.). A quality of raw sequencing data was controlled using FastQC. After adapter and low quality reads (<Q20) were removed using FASTX_Trimmer and BBMap, trimmed reads were mapped to the reference genome using TopHat. Gene expression levels were estimated using Fragments Per kb per Million reads (FPKM) values by Cufflinks. The FPKM values were normalized on the basis of quantile normalization method using EdgeR within R. Gene-set enrichment analysis (GSEA) was conducted using GSEA software v4.2.3 with the "log2_Ratio_of_Classes" metric to generate a ranked list and a "phenotype" permutation type. Gene sets that contain fewer than 50 genes and more than 500 were excluded in the analysis.

For microarray, total RNA was extracted from MDA-MB-231 control or *NR1D1* KO cells treated with 200 μmol/L H_2O_2 for 72 hours. cDNA was synthesized using the GeneChip Whole Transcript amplification kit as described by the manufacturer. The sense cDNA was then fragmented and biotin-labeled with terminal deoxynucleotidyl transferase using the GeneChip Whole Transcript terminal labeling kit. Approximately 5.5 μg of labeled DNA target was hybridized to the Affymetrix GeneChip Human Gene 2.0 ST Array at 45°C for 16 hours. Hybridized arrays were washed and stained on a GeneChip Fluidics Station 450 and scanned on a GCS3000 Scanner (Affymetrix). The probe cell intensity data computation and a CEL file generation was performed using Affymetrix GeneChip Command Console Software. Gene ontology term analysis was performed using DAVID 2021 software (https://david.ncifcrf.gov/). Protein–protein interaction network analysis was performed using STRING v11.5 database (http://string-db.org).

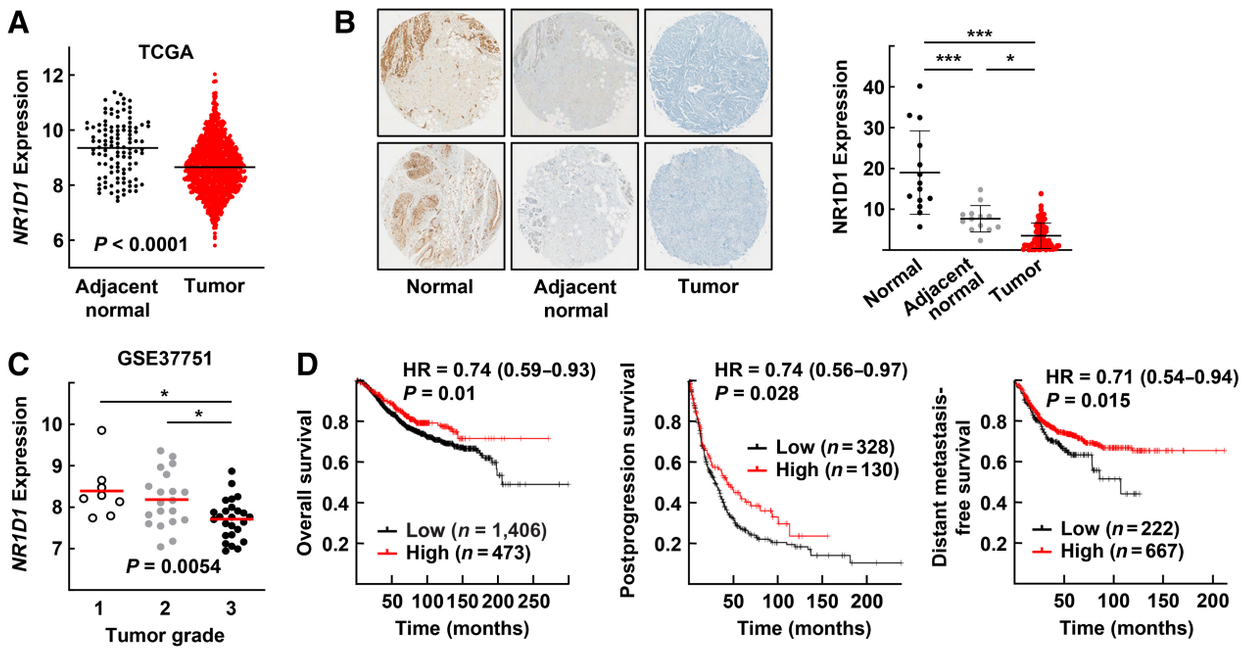

Figure 1.

High NR1D1 expression is correlated with improved clinical outcomes in patients with breast cancer. **A,** Expression level of *NR1D1* in breast cancer ($n = 1073$) and adjacent normal ($n = 112$) tissues from TCGA database was analyzed using the Breast Cancer Integrative Platform (BCIP; http://www.omicsnet.org/bcancer/). Bars indicate the median expression level in each group. Statistical analysis was performed using the Mann–Whitney *U* test. **B,** Breast carcinoma ($n = 75$), adjacent normal ($n = 13$), and normal ($n = 14$) breast tissue sections were subjected to immunostaining with anti-NR1D1 antibody. Left, representative images from each group are shown. Staining intensities were quantified and statistical analysis was performed using one-way ANOVA followed by Tukey post hoc test. *, $P < 0.05$; ***, $P < 0.001$. **C,** Expression level of *NR1D1* was analyzed in different grades of breast cancer specimens from the GSE37751 dataset obtained from the NCBI GEO website. Bars indicate the median expression level in each group. Statistical analysis was performed using one-way ANOVA followed by Tukey post hoc test. *, $P < 0.05$. **D,** Prognostic value of NR1D1 in breast cancer was analyzed using the Kaplan–Meier Plotter database (http://kmplot.com/analysis/), which integrates multiple GEO datasets. Overall survival and postprogression survival were analyzed in all patients with breast cancer. Distant metastasis-free survival was analyzed in patients with lymph node–positive breast cancer (889 patients were lymph node-positive out of 1,909 patients with breast cancer). Log-rank tests were performed. HR below 1 implies greater survival probabilities for the high-*NR1D1* expression group compared with the low-*NR1D1* expression group. Detailed information on tumor samples can be found in the individual GEO dataset in the NCBI GEO website.

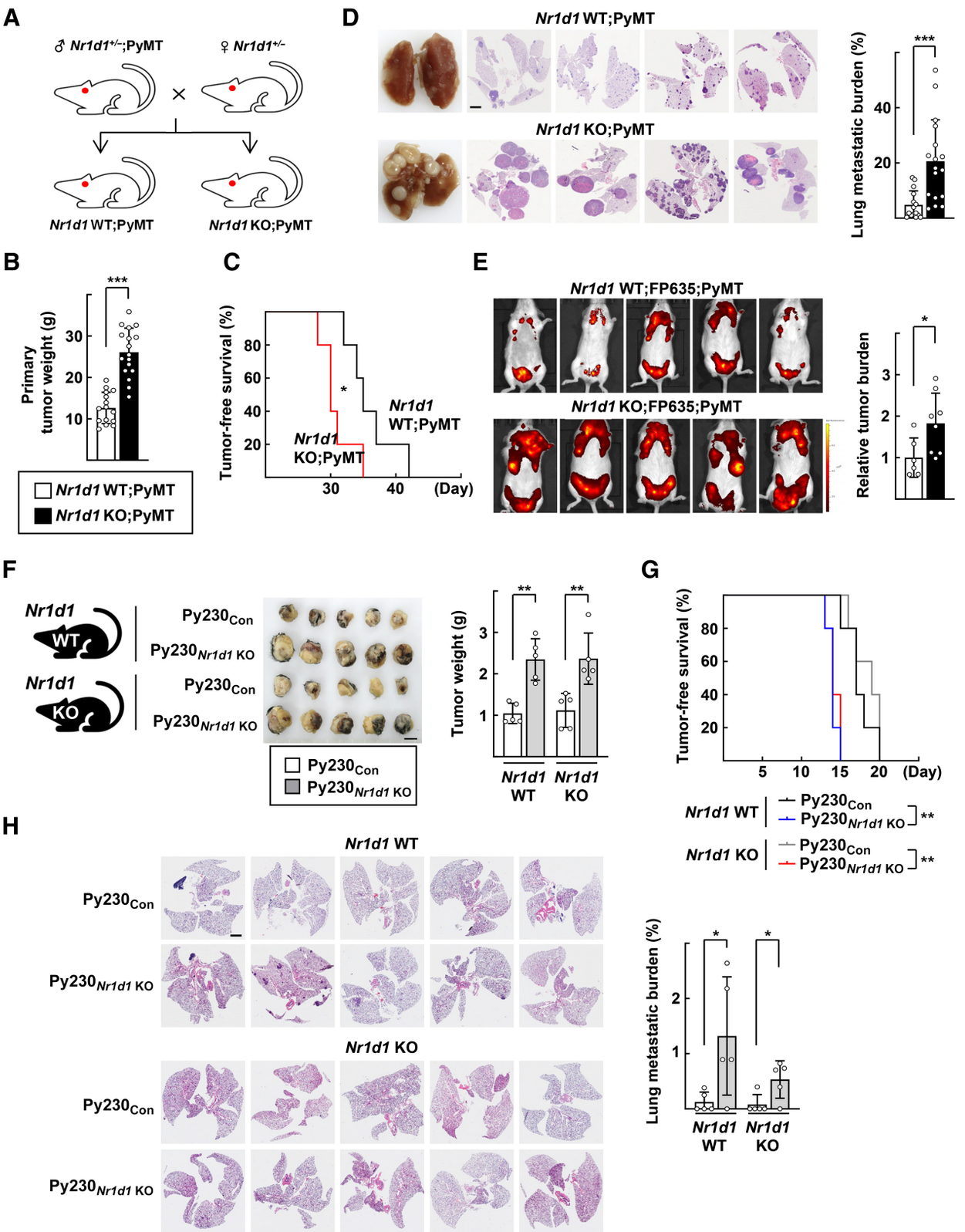
A
♂ Nr1d1+/−;PyMT
♀ Nr1d1+/−
Nr1d1 WT;PyMT
Nr1d1 KO;PyMT
B
Primary tumor weight (g)
***
Nr1d1 WT;PyMT
Nr1d1 KO;PyMT
C
Tumor-free survival (%)
Nr1d1 WT;PyMT
Nr1d1 KO;PyMT
(Day)
D
Nr1d1 WT;PyMT
Nr1d1 KO;PyMT
Lung metastatic burden (%)
E
Nr1d1 WT;FP635;PyMT
Nr1d1 KO;FP635;PyMT
Relative tumor burden
F
Nr1d1 WT
Nr1d1 KO
Py230Con
Py230Nr1d1 KO
Tumor weight (g)
G
Tumor-free survival (%)
(Day)
Nr1d1 WT
Nr1d1 KO
Lung metastatic burden (%)
H
Nr1d1 WT
Nr1d1 KO

Examination of tumor tissues

Paraffin-embedded tumor tissues were cut into 4–μm sections and mounted onto silane-coated glass slides. To visualize cytosolic DNA, PicoGreen staining was performed using Quant-iT PicoGreen dsDNA Assay Kit (Thermo Fisher Scientific; ref. 15). Briefly, after deparaffinization and antigen retrieval, slides were subjected to staining with PicoGreen dsDNA reagent together with Alexa Fluor 594-conjugated wheat germ agglutinin (WGA), which labels plasma membrane. The slides were mounted and analyzed using a confocal microscope (Carl Zeiss LSM710). For IHC, sections of paraffin-embedded tissues were subjected to staining using specific antibodies (Supplementary Table S1). Quantification was performed using whole-slide scan images by Vectra Polaris Automated Quantitative Pathology Imaging System and inForm software (Akoya Biosciences). Representative images were obtained using a brightfield microscopy with a 40× objective lens (Olympus, BX53).

For flow cytometry, tumor tissues were dissociated into single cells using the Tumor Dissociation Kit (#130–096–730) and the gentleMACS Octo Dissociator (Miltenyi Biotec). For staining of surface antigens, single cells were resuspended and incubated for 30 minutes at 4°C with specific antibodies shown in Supplementary Table S1. For staining of intracellular proteins, cells were fixed and permeabilized using a transcription factor buffer set (BD Pharmingen), and stained with specific antibodies (Supplementary Table S1). Cells were acquired on flow cytometry (LSR Fortessa, BD Biosciences) and analyzed by FlowJo software (TreeStar, Tree Star Inc.).

Western blotting, ELISA, and immunofluorescence

For Western blotting, cells were lysed in lysis buffer (50 mmol/L Tris-HCl pH 7.4, 150 mmol/L NaCl, 5 mmol/L EDTA, 1% NP-40, protease inhibitor, and phosphatase inhibitor) and incubated on ice for 30 minutes. After centrifugation, the supernatants were collected, and protein concentrations were measured using BCA assay (15, 29). Equal amounts of proteins were separated on SDS-PAGE, followed by semi-dry transfer onto polyvinylidene difluoride membrane (Millipore). The membranes were blocked with 5% BSA or 5% nonfat milk in 0.1% PBST, and then primary antibodies were exposed overnight at 4°C. Secondary horseradish peroxidase–conjugated antibodies were exposed for 1 hour at room temperature (Supplementary Table S1). Detection was performed using Amersham ECL Western Blotting Detection Reagent (Cytiva). Band intensities of proteins were quantified with ImageJ software. The level of cGAMP in mammary tumor tissues was measured using 2′3′-cGAMP ELISA kit (#501700, Cayman Chemical). The amounts of proteins in culture supernatants were measured using commercially available ELISA kits [IFNα and IFNβ (MBS2506739 and MBS2513798, respectively; MyBioSource), CCL5 and CXCL10 (DRN00B and DIP100, respectively; R&D Systems)]. For immunofluorescence staining, cells were fixed with acetone, blocked with 5% BSA in PBS, and then incubated with a primary antibody at 4°C overnight. Cells were incubated with Alexa Fluor 488–conjugated secondary antibody for 1 hour at room temperature and stained with 4′,6-diamidino-2-phenylindole (DAPI; Supplementary Table S1; ref. 30). Images were analyzed using a confocal microscope (Carl Zeiss LSM710).

Statistical analyses

Statistical analyses were performed using GraphPad Prism 9 software. Experimental results are given as the mean ± SD, unless indicated otherwise. Statistically significant differences were determined using the nonparametric Mann–Whitney *U* test (two-tailed) or the unpaired Student *t* test, as indicated in figure legends. $P < 0.05$ was considered statistically significant.

Data availability

The RNA-seq and microarray data generated in this study are deposited in GEO at GSE222645 and GSE231652, respectively. TCGA database was obtained and analyzed in the Breast Cancer Integrative Platform (BCIP; http://www.omicsnet.org/bcancer/). The GSE37751 dataset was downloaded from GEO (http://www.ncbi.nlm.nih.gov/geo/). Kaplan–Meier plotter mRNA breast cancer database (http://kmplot.com/analysis/) was utilized to assess the prognostic value of NR1D1 in breast cancer. All other raw data are available upon request from the corresponding author.

Results

High NR1D1 expression is associated with better clinical outcomes in patients with breast cancer

To assess the clinical implications of NR1D1, we first analyzed the expression level of *NR1D1* in breast cancer and adjacent normal tissues using TCGA database. The expression level of *NR1D1* in breast cancer tissues was significantly lower than that in adjacent normal tissues ($P < 0.0001$; **Fig. 1A**). Consistently, immunostaining of NR1D1 protein in tissue microarray showed that NR1D1 level in tumor tissues was lower than that in normal and adjacent normal tissues (**Fig. 1B**). Analysis of the GSE37751 dataset showed that the expression level of *NR1D1* was inversely correlated with tumor grade in patients with breast cancer (**Fig. 1C**). We previously reported that high NR1D1 expression is correlated with improved clinical outcomes in patients with breast cancer who received chemotherapy (24, 31). We analyzed the prognostic value of NR1D1 in breast cancer more thoroughly using the Kaplan–Meier plotter database, which integrates tumor samples from multiple GEO datasets. Survival analyses of patients with breast cancer showed that overall survival and postprogression survival were improved in the high-*NR1D1* expression group compared with the low-*NR1D1* expression group (**Fig. 1D**). Furthermore, the high expression of

Figure 2.

Mammary tumor progression and lung metastasis are enhanced in the absence of *Nr1d1* in tumor cells. **A,** Schematic representation of the strategy to generate *Nr1d1* KO;PyMT mice. **B,** Quantification of mammary gland tumor weight from 14-week-old *Nr1d1* WT;PyMT ($n = 15$) and *Nr1d1* KO;PyMT ($n = 17$) mice. Mann–Whitney *U* test. ***, $P < 0.001$. **C,** Kaplan–Meier tumor-free survival curve for *Nr1d1* WT;PyMT ($n = 5$) and *Nr1d1* KO;PyMT ($n = 5$) mice. Log-rank test. *, $P < 0.05$. **D,** Representative image of lung tissues and histologic analysis of lung metastasis from 14-week-old *Nr1d1* WT;PyMT and *Nr1d1* KO;PyMT mice. Scale bar, 2 mm (left). Quantification of tumor burden in lung tissues from 14-week-old *Nr1d1* WT;PyMT ($n = 15$) and *Nr1d1* KO;PyMT ($n = 17$) mice. Mann-Whitney *U* test. ***, $P < 0.001$. **E,** Left, representative mouse fluorescence images of 14-week-old *Nr1d1* WT;FP635;PyMT and *Nr1d1* KO;FP635;PyMT mice using an In Vivo Imaging System. Right, quantification of fluorescence signals over tumor region ($n = 6$ for *Nr1d1* WT;FP635;PyMT and $n = 8$ for *Nr1d1* KO;FP635;PyMT). Mann–Whitney *U* test. *, $P < 0.05$. **F,** Left, representative tumor images after orthotopic injection of control or *Nr1d1* KO-Py230 cells into the *Nr1d1* WT and *Nr1d1* KO C57BL/6 mice. Scale bar, 1 cm. Right, quantification of mammary gland tumor weight ($n = 5$ per group). Mann–Whitney *U* test. **, $P < 0.01$. **G,** Kaplan–Meier tumor-free survival curve for the indicated group of allografted mice ($n = 5$ per group). Log-rank test. **, $P < 0.01$. **H,** Left, histologic analysis of lung metastasis from the indicated group of allografted mice. Right, quantification of tumor burden in lung tissues ($n = 5$ per group). Unpaired Student *t* test. *, $P < 0.05$.

NR1D1 was associated with improved distant metastasis-free survival, particularly in patients with lymph node–positive breast cancer, indicating the involvement of NR1D1 in breast cancer progression and metastasis (**Fig. 1D**). These data suggest that high NR1D1 expression has a favorable impact on patient outcomes and may be an important prognostic factor in patients with breast cancer.

Breast cancer growth and lung metastasis are enhanced in the absence of *Nr1d1*

To elucidate the role of NR1D1 in the progression of breast cancer, we generated a genetically mutated mouse line lacking the *Nr1d1* gene using the CRISPR-Cas9 system (Supplementary Fig. S1A–S1D). The mouse line was crossbred with MMTV–PyMT mice, which is an aggressive mammary adenocarcinoma model that develops invasive carcinoma and pulmonary metastasis (**Fig. 2A**; ref. 32). We observed that mammary gland tumor weight was significantly higher in *Nr1d1* KO;PyMT mice than in *Nr1d1* WT;PyMT mice (**Fig. 2B**). The tumor-free survival rate was lower in *Nr1d1* KO;PyMT mice compared with control mice (**Fig. 2C**). Furthermore, the lung metastatic burden was higher in *Nr1d1* KO;PyMT mice than in control mice (**Fig. 2D**). When monitoring tumor burden in living *Nr1d1*;FP635;PyMT mice, fluorescence indicating tumors was observed in both the mammary glands and lungs of 14-week-old mice. The intensity was higher in *Nr1d1* KO;FP635;PyMT mice compared with *Nr1d1* WT;FP635;PyMT mice (**Fig. 2E**). These results show that NR1D1 deficiency affects the growth and metastatic ability of mammary gland tumors.

Because we used the systemic *Nr1d1* KO strategy, we wanted to determine whether the altered tumor progression associated with NR1D1 was due to NR1D1 in tumor cells or in other components such as immune cells in the TME. To this end, we used a syngeneic orthotopic transplant mouse model with *Nr1d1*-deficient Py230, which was derived from a PyMT C57BL/6 female mouse, *Nr1d1* KO-Py230 (33). Control and *Nr1d1* KO-Py230 cells were implanted into the mammary fat pads of *Nr1d1* WT or KO C57BL/6 mice. *Nr1d1* KO-Py230 tumors were larger than Py230 control tumors in both *Nr1d1* WT and KO C57BL/6 mice (**Fig. 2F**). The tumor-free survival rate was lower in *Nr1d1* KO-Py230—implanted mice than in control-Py230–implanted mice (**Fig. 2G**). Furthermore, *Nr1d1* KO-Py230 tumors showed a higher degree of lung metastasis than Py230 control tumors (**Fig. 2H**). However, *Nr1d1* expression in the host had no significant effects on tumor growth and lung metastasis (**Fig. 2F–H**). These results indicate that NR1D1 loss in cancer cells induces an increase in mammary tumor growth and metastasis.

NR1D1 enhances cGAS/STING signaling–mediated antitumor immunity

To understand the molecular function of NR1D1, we analyzed the global gene expression pattern in mammary tumors from *Nr1d1* KO;PyMT mice and their control littermates by RNA-seq. We identified a strong differential pattern: that is, a total of 818 genes were significantly upregulated, whereas 1,325 genes were downregulated in the *Nr1d1* KO;PyMT mammary tumors compared with control tumors (**Fig. 3A** and **B**; Supplementary Fig. S2A). Gene Ontology biological process (GOBP) revealed that the most enriched gene set was signal transduction in response to DNA damage, consistent with our previous observation of the role of NR1D1 in the regulation of DDR (**Fig. 3C**; ref. 24). Notably, the top 10 GOBP enriched in *Nr1d1* WT;PyMT tumors included regulation of T cell–mediated immunity and T-cell proliferation and activation (**Fig. 3C** and **D**; Supplementary Fig. S2B). To elucidate the role of NR1D1 in cancer cells, we established *NR1D1* KO-MDA-MB-231 sublines using the CRISPR-Cas9 system (Supplementary Fig. S2C). We analyzed alteration of global gene expression pattern in the *NR1D1* KO cells. Depletion of *NR1D1* induced a marked shift in the transcriptomic profile, with a total of 326 genes significantly upregulated and 501 genes downregulated (**Fig. 3E**). Gene Ontology enrichment analyses showed that the biological processes of inflammatory responses and innate immune responses were significantly downregulated by depleting *NR1D1* (**Fig. 3F**; Supplementary Fig. S2D). The STRING-generated interaction network revealed interactive clusters, such as the cytosolic DNA-sensing pathway, response to type I IFN, and regulation of T-cell activation (**Fig. 3G**). These results suggest that NR1D1 may have a role in type I IFN–mediated immune activation during the progression of breast cancer.

Therefore, we hypothesized that NR1D1-induced DNA repair impairment leads to the activation of cGAS-STING signaling and T cell–mediated immunity. To test this hypothesis, we first evaluated the degree of DNA repair by γH2AX staining in the tumor sections from *Nr1d1* KO;PyMT mice and control mice. Consistent with our previous report, the number of γH2AX-positive cells was lower in the mammary glands and lung-metastasized tumors of *Nr1d1* KO;PyMT than control mice (**Fig. 4A**; ref. 24). The differences were not observed in the mammary glands of *Nr1d1* KO and control mice without crossing to the PyMT model, suggesting that NR1D1 may affect DDR particularly under conditions of DNA damage (Supplementary Fig. S3A). The level of PicoGreen-stained cytosolic DNA was lower in the tumors of *Nr1d1* KO;PyMT mice than control mice (**Fig. 4B**). The amount of cGAMP, produced by cGAS in response to cytosolic DNA, was lower in *Nr1d1* KO;PyMT tumors compared with control tumors (**Fig. 4C**). The levels of phosphorylated STING (pSTING), IFNα, and IFNβ were lower in the tumors of *Nr1d1* KO;PyMT mice than control mice (**Fig. 4D**; Supplementary Fig. S3B). Next, we examined the immune status of the TME including immune infiltration in the mouse model. Significant decreases in the numbers of infiltrated $CD3^+$ T lymphocytes, $CD8^+$ T cells, and intratumoral $NK1.1^+$ NK cells were observed in the mammary and lung metastatic tumors of *Nr1d1* KO;PyMT mice (**Fig. 5A**). Consistent with IHC data, flow cytometry showed a significant decrease in the percentages of $CD3^+$ T lymphocytes, $CD8^+$ T cells and NK cells, and a higher $CD4^+/CD8^+$ ratio in *Nr1d1* KO;PyMT tumors compared with control tumors (**Fig. 5B**; Supplementary Fig. S4). However, the relative numbers of tumor-associated neutrophils (TAN), tumor-associated macrophages (TAM), and regulatory T cells (Treg) were higher in *Nr1d1* KO;PyMT than in *Nr1d1* WT;PyMT tumors (**Fig. 5B**). Analyses of tumor tissues from Py230 orthotopic allografted mice showed that the expression of pSTING and IFNβ, and infiltration of $CD8^+$ T cells were lower in *Nr1d1* KO-Py230 tumors, irrespective of *Nr1d1* expression in the host mice, confirming the importance of *Nr1d1* in tumor cells (Supplementary Fig. S5). Taken together, these data suggest that NR1D1 deficiency induces DNA damage–induced cGAS-STING signaling pathway in mammary gland and lung metastatic tumors, which promote antitumor immunity.

NR1D1 activates type I IFN responses through cytosolic DNA-induced cGAS-STING signaling

To demonstrate the direct role of NR1D1 in inducing STING signaling, we analyzed DDR and STING signaling in the *NR1D1* KO-MDA-MB-231 cells. First, we confirmed the role of NR1D1 in DNA repair by showing that the number of oxidative stress–induced γH2AX foci was far less in *NR1D1* KO cells compared with control cells (**Fig. 6A**; ref. 24). The level of cytosolic DNA increased consistently after hydrogen peroxide (H_2O_2) or doxorubicin treatment of the control cells but was lower in the *NR1D1* KO cells (**Fig. 6B**).

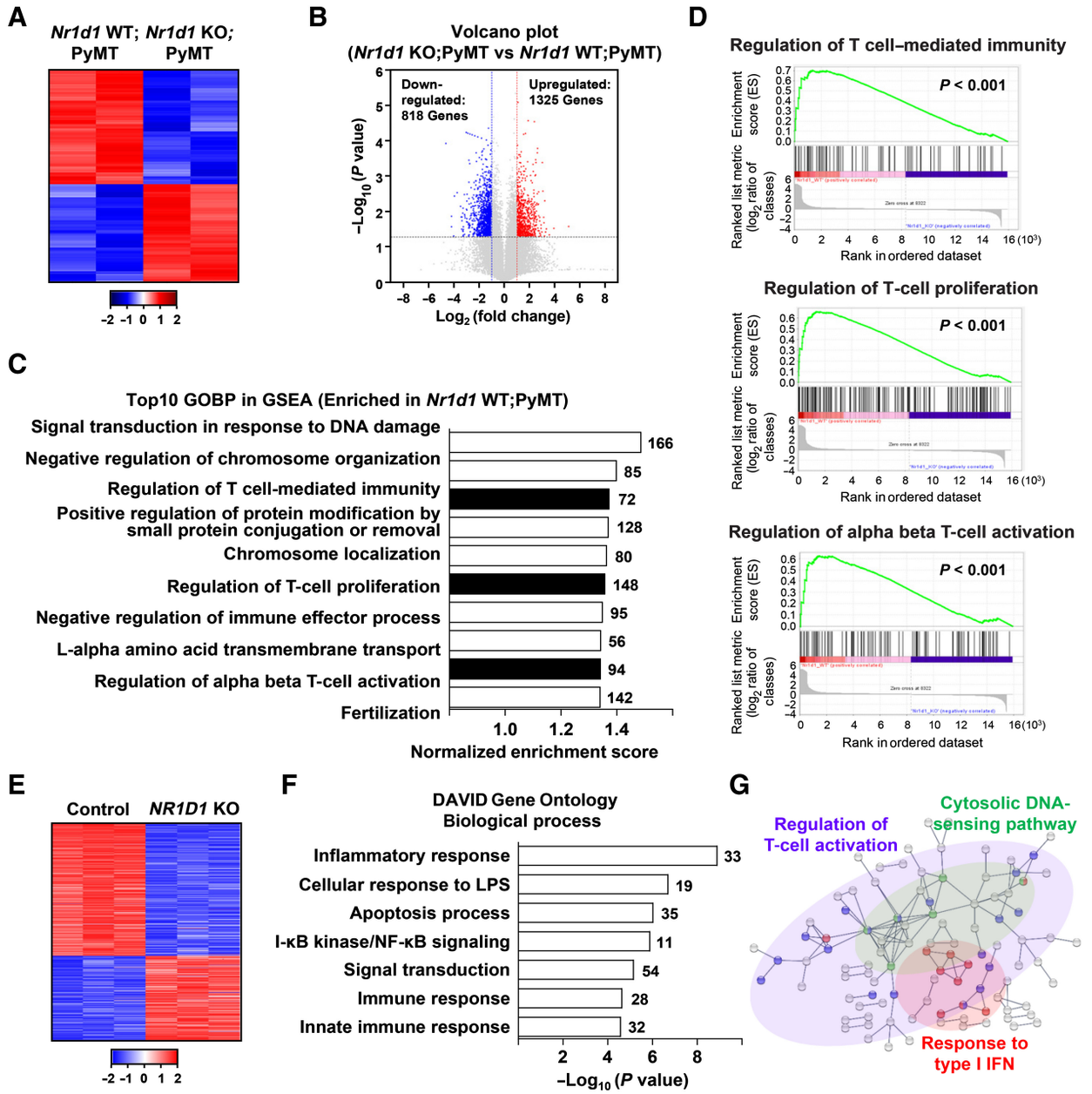

Figure 3.

Biological processes including type I IFN signaling and T cell–mediated immune responses are associated with NR1D1. **A,** Heat map of differentially expressed genes (|FC| ≥ 2 and $P < 0.05$) in the mammary gland tumors between 14-week-old *Nr1d1* WT;PyMT and *Nr1d1* KO;PyMT mice using RNA-seq data. **B,** Volcano plot of differentially expressed genes. Red and blue dots show upregulated and downregulated genes in *Nr1d1* KO;PyMT mice, respectively. **C,** GSEA showing the top 10 enriched biological processes in *Nr1d1* WT;PyMT mammary tumors compared with *Nr1d1* KO;PyMT mammary tumors based on normalized enrichment score. The number of annotated genes in each ontology is shown at the right side of the bar. **D,** GSEA enrichment plots of representative gene sets positively correlated with *Nr1d1* WT;PyMT mammary tumors (vs. *Nr1d1* KO;PyMT mammary tumors). **E,** MDA-MB-231 control or *NR1D1* KO cells were treated with 200 μmol/L H_2O_2 for 72 hours. RNA was extracted and subjected to microarray analysis. Heat map of differentially expressed genes (|FC| ≥ 1.5 and $P < 0.05$) is shown. **F,** DAVID Gene Ontology analysis of differentially expressed genes showing top 7 downregulated biological process in *NR1D1* KO cells compared with control cells based on *P* value. The number of annotated genes in each ontology is shown at the right side of the bar. **G,** An interaction network of differentially expressed genes obtained by the STRING database. Genes included in GOBP of "type I IFN signaling pathway" and "regulation of T-cell activation," and Kyoto Encyclopedia of Genes and Genomes (KEGG) pathway of "cytosolic DNA-sensing pathway" are colored.

Phosphorylation of STING and its downstream proteins, such as TBK1 and IRF3, increased after H_2O_2 or doxorubicin treatment of control but not *NR1D1* KO cells (**Fig. 6C**; Supplementary Fig. S6A). We also found that the levels of IFNα, IFNβ, CCL5, and CXCL10 were increased after H_2O_2 or doxorubicin treatment of control cells, but were barely increased in *NR1D1* KO cells (**Fig. 6D**; Supplementary Fig. S6B). The levels of chemokines induced by cisplatin were lower in the *NR1D1* KO cells compared with control cells (Supplementary

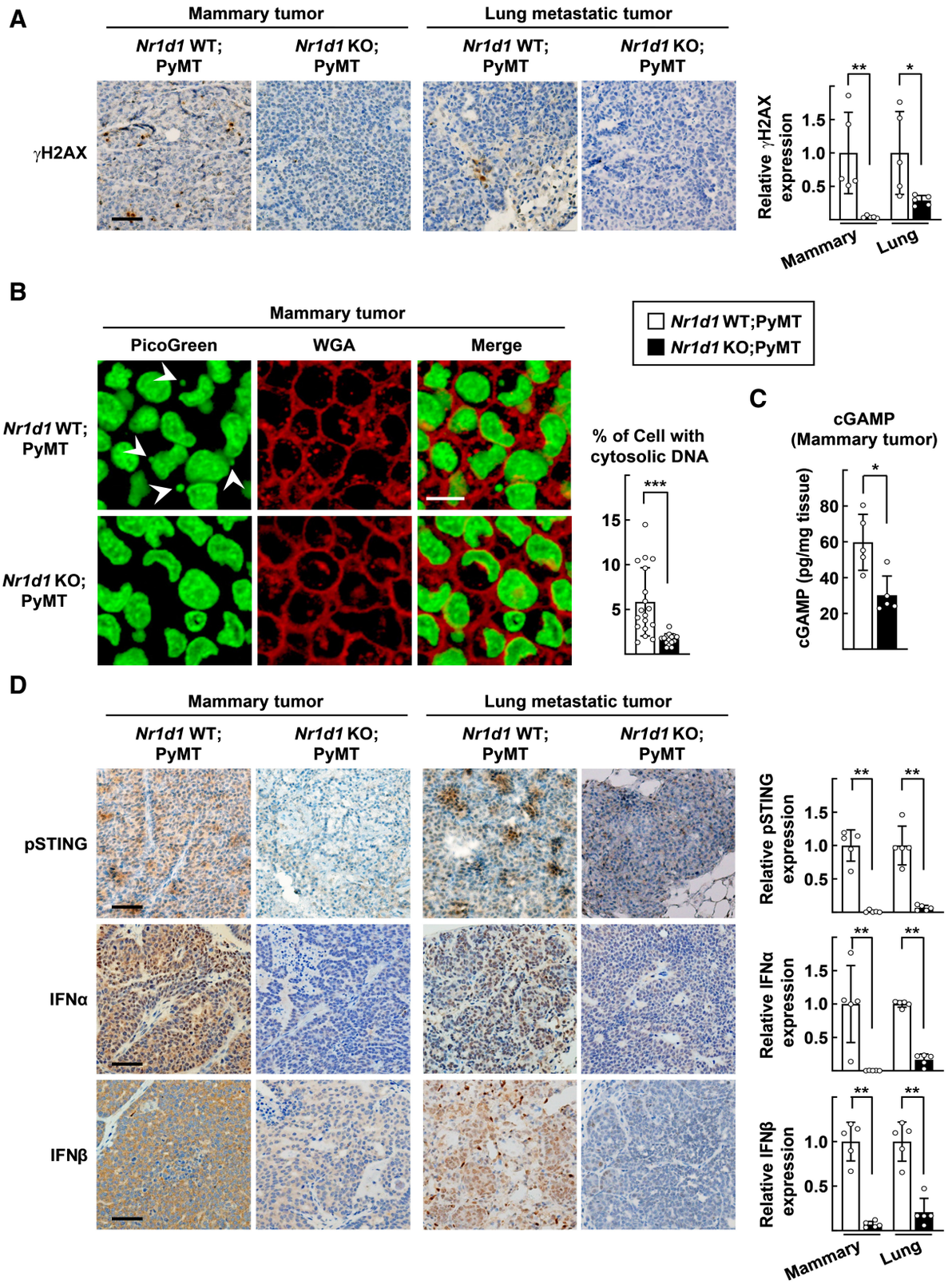
A
Mammary tumor
Lung metastatic tumor
Nr1d1 WT; PyMT
Nr1d1 KO; PyMT
γH2AX
Relative γH2AX expression
Mammary
Lung
B
Mammary tumor
PicoGreen
WGA
Merge
Nr1d1 WT;PyMT
Nr1d1 KO;PyMT
% of Cell with cytosolic DNA
C
cGAMP (Mammary tumor)
cGAMP (pg/mg tissue)
D
pSTING
IFNα
IFNβ
Relative pSTING expression
Relative IFNα expression
Relative IFNβ expression

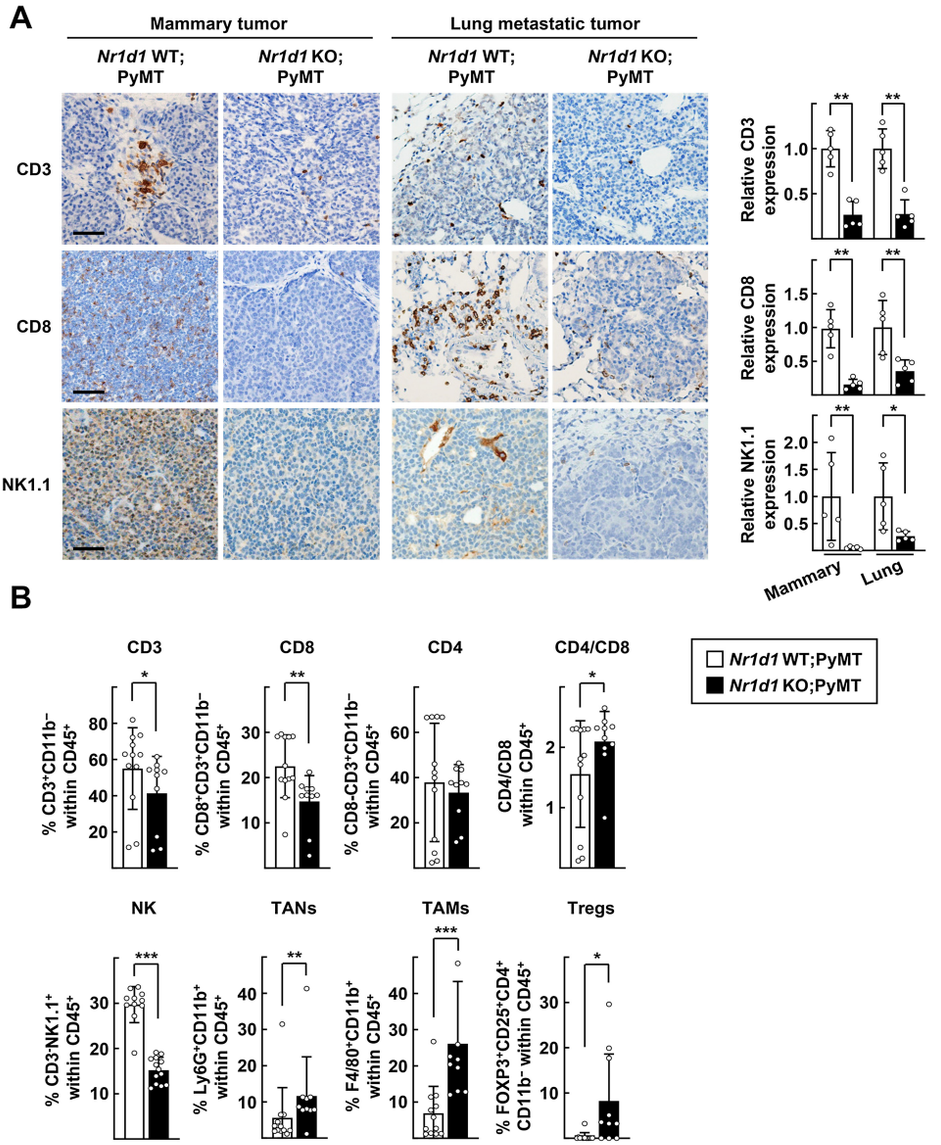

Figure 5.

Recruitment of $CD8^+$ T cells and NK cells was decreased in the mammary tumors of *Nr1d1* KO;PyMT mice. **A,** IHC analysis of CD3, CD8, and NK1.1 in mammary gland and lung tissues from 14-week-old *Nr1d1* WT;PyMT and *Nr1d1* KO;PyMT mice. Left, representative images from each group are shown. Scale bars, 50 μm. Right, staining intensities were quantified from five tumor samples from each group. Mann–Whitney *U* test. *, $P < 0.05$; **, $P < 0.01$. **B,** The percentage of T cells ($CD3^+CD11b^-$ within $CD45^+$), CD8 ($CD8^+CD3^+CD11b^-$ within $CD45^+$), CD4 ($CD8^-CD3^+CD11b^-$ within $CD45^+$), the CD4/CD8 ratio, NK ($CD3^-NK1.1^+$ within $CD45^+$), TANs ($Ly6G^+CD11b^+$ within $CD45^+$), TAMs ($F4/80^+CD11b^+$ within $CD45^+$), and Tregs ($FOXP3^+CD25^+CD4^+CD11b^-$ within $CD45^+$) in 10-week-old *Nr1d1* WT;PyMT and *Nr1d1* KO;PyMT mice. T cells, CD8, CD4, TANs, TAMs, and Tregs were analyzed from same samples ($n = 12$ for *Nr1d1* WT;PyMT and $n = 10$ for *Nr1d1* KO;PyMT). NK cells were analyzed from independent samples ($n = 11$ for *Nr1d1* WT;PyMT and $n = 13$ for *Nr1d1* KO;PyMT). Mann–Whitney *U* test. *, $P < 0.05$; **, $P < 0.01$; ***, $P < 0.001$.

Fig. S6B). Depletion of cGAS or STING attenuated the H_2O_2-induced expression of chemokines, indicating that the effects were cGAS/STING dependent (Supplementary Fig. S6C). The SKBR3 sublines that lacked *NR1D1* showed similar results (Supplementary Fig. S7A–S7D). Taken together, these results show that NR1D1 activates DNA damage–induced STING signaling in breast cancer cells.

GSK4112 and SR9009, NR1D1 agonists, activate type I IFN signaling that induces antitumor immunity *in vitro* and *in vivo*

The function of NR1D1 is modulated by its ligands; therefore, we examined the effects of GSK4112 and SR9009, two well-known NR1D1 ligands, on the activation of STING-mediated type I IFN signaling in mammary tumors (34). Treatment with these ligands increased the

Figure 4.

Cytosolic DNA and STING signaling are suppressed in the mammary tumor of *Nr1d1* KO;PyMT mice. **A,** IHC analysis of γH2AX in mammary gland and lung tissues from 14-week-old *Nr1d1* WT;PyMT and *Nr1d1* KO;PyMT mice. Left, representative images from each group are shown. Scale bar, 50 μm. Right, staining intensities were quantified from five tumor samples from each group. Mann–Whitney *U* test. *, $P < 0.05$; **, $P < 0.01$. **B,** Cytosolic DNA staining in mammary tumor tissues from 14-week-old *Nr1d1* WT;PyMT and *Nr1d1* KO;PyMT mice. Left, tumor sections were stained with PicoGreen dsDNA reagent (green) and wheat germ agglutinin (WGA) that labels plasma membrane (red). Arrowheads, cytosolic DNA. Scale bar, 10 μm. Right, the number of cells with cytosolic DNA was counted from at least 100 cells for each sample and is presented as percentage of total counted cells. Three tumor samples from each group and five random fields per sample were analyzed. Mann–Whitney *U* test. ***, $P < 0.001$. **C,** The level of cGAMP in mammary tumor tissues from 14-week-old *Nr1d1* WT;PyMT and *Nr1d1* KO;PyMT mice measured by ELISA ($n = 5$ per group). Mann–Whitney *U* test. *, $P < 0.05$. **D,** IHC analysis of pSTING, IFNα, and IFNβ in mammary gland and lung tissues from 14-week-old *Nr1d1* WT;PyMT and *Nr1d1* KO;PyMT mice. Left, representative images from each group are shown. Scale bar, 50 μm. Right, staining intensities were quantified from five tumor samples from each group. Mann–Whitney *U* test. **, $P < 0.01$.

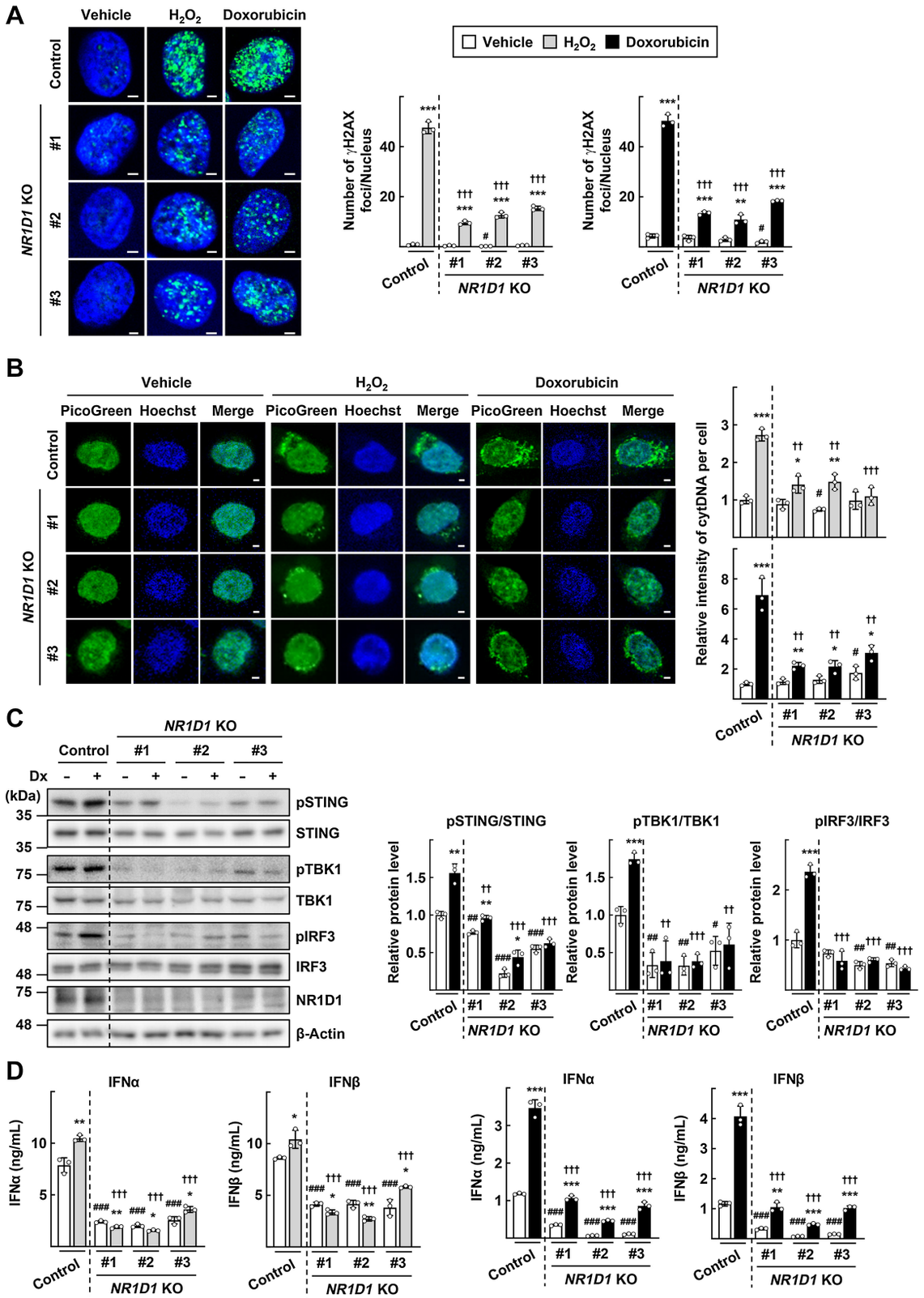
A
Vehicle
H2O2
Doxorubicin
Control
NR1D1 KO
#1
#2
#3
Number of γH2AX foci/Nucleus
B
PicoGreen
Hoechst
Merge
Relative intensity of cytDNA per cell
C
Dx
(kDa)
pSTING
STING
pTBK1
TBK1
pIRF3
IRF3
NR1D1
β-Actin
pSTING/STING
pTBK1/TBK1
pIRF3/IRF3
Relative protein level
D
IFNα
IFNβ
IFNα (ng/mL)
IFNβ (ng/mL)

expression of type I IFNs, CCL5, and CXCL10 in MDA-MB-231 cells, but expression was lower in *NR1D1* KO-MDA-MB-231 cells (Supplementary Fig. S8). These results demonstrated that GSK4112 and SR9009 increased STING-mediated type I IFN production in an NR1D1-dependent manner. Administration of SR9009 (100 mg/kg) significantly delayed tumor onset and reduced tumor weight in *Nr1d1* WT;PyMT mice, whereas it did not have this effect on *Nr1d1* KO;PyMT mice (**Fig. 7A**). Lung metastatic burden and the numbers of metastatic nodules and were markedly reduced in *Nr1d1* WT;PyMT mice but not in *Nr1d1* KO;PyMT mice after administration of SR9009 (**Fig. 7B**). IHC staining showed that the number of cells with γH2AX foci, pSTING, IFNα, or IFNβ increased in the SR9009-treated group only in *Nr1d1* WT;PyMT mice (**Fig. 7C**; Supplementary Fig. S9). Furthermore, administration of SR9009 promoted tumor infiltration of $CD3^+$ T cells, $CD8^+$ T cells, and NK cells in *Nr1d1* WT;PyMT mice, but not in *Nr1d1* KO;PyMT mice (**Fig. 7C**; Supplementary Fig. S9). These results indicate that NR1D1 agonists enhance type I IFN–mediated antitumor immunity in an NR1D1-dependent manner.

Discussion

To date, several mechanisms underlying the antitumor effect of NR1D1 have been suggested in various cancer types. Activation of NR1D1 by synthetic agonists cause cancer cell death by suppressing *de novo* lipogenesis and autophagy in breast cancer, melanoma, and small-cell lung cancer (23, 35). NR1D1 suppresses the growth of ovarian cancer cells by inhibiting the JAK/STAT3 signaling pathway (36). However, these studies had limitations in exploring the immune system since the antitumor effects of NR1D1 were examined in a xenograft model with immunodeficient mice. Here, we explored the role of NR1D1 in spontaneous tumors that developed in MMTV–PyMT mice with an intact immune system. We demonstrated that deletion of *Nr1d1* markedly suppressed immune cell infiltration and activation, accompanied by enhanced tumor growth and metastasis. In line with our previous findings that NR1D1 inhibits DNA repair against DNA damage induced by oxidative stress or DNA-damaging agents (24, 37), NR1D1 probably elicited antitumor T-cell response by inhibiting DNA repair. Because the mechanism of NR1D1 in inhibiting DNA repair involves its recruitment to DSB sites, thereby hindering the recruitment of DDR factors, NR1D1 might also have a nongenomic function aside from its genomic transcriptional repressor function. The coregulation of genomic and nongenomic actions are crucial and common for the full response of nuclear receptors, such as steroid hormone, thyroid, and retinoic acid receptors (38–40). Interestingly, NR1D1-induced type I IFN expression was observed only in breast cancer cells but not in MCF10A nontumorigenic breast epithelial cells (Supplementary Fig. S10). In addition, the level of γH2AX in normal mammary gland was not significantly different between *Nr1d1* WT and KO mice, contrary to what observed in the tumor sections of *Nr1d1* WT;PyMT and KO;PyMT mice (Supplementary Fig. S3A). Cancer cells are highly burdened by genomic instability and replication stress, which cause genome-wide DNA damage; therefore, the role of NR1D1 in inhibiting DNA repair is predominant in cells with hyperdependent on DDR signaling, especially breast cancer cells with mutations of *BRCA1/2, ATM*, and tumor protein 53.

As the activity of NR1D1 is modulated by ligands, specific ligands that pharmacologically target this nuclear receptor have been explored in various pathologic conditions including sleep disorders, inflammatory diseases, metabolic disorders, and cancer (23, 35, 41, 42). The first synthetic ligand for NR1D1, GSK4112, has been widely used as an *in vitro* probe of NR1D1 function, but it has limited *in vivo* exposure due to its poor pharmacokinetic properties (43). SR9009 and SR9011 have shown as promising pharmaceutical agents with potent *in vivo* activities (41). However, the specificity of SR9009 on NR1D1 regarding the cytotoxic effects on cancer cells has been controversial. Studies have demonstrated that SR9009 exerts antitumor effects through the NR1D1-mediated repression of downstream genes in multiple cancer types including glioblastoma, small-cell lung cancer, and breast cancer (23, 35). However, Dierickx and colleagues (2019) demonstrated that SR9009 reduced the viability of cancer cells and embryonic stem cells in an NR1D1-independent manner, although the mechanisms remain unknown (44). In our study, the antitumor effects of SR9009 were abolished upon administrated in *Nr1d1* KO;PyMT mice, accompanied by the inactivation of STING signaling and aborted recruitment of $CD8^+$ T cells and NK cells, demonstrating the NR1D1-dependent action of SR9009 (**Fig. 7**). We speculate that SR9009 exerts its antitumor effects through NR1D1-mediated DNA repair inhibition, since our previous study showed that GSK4112 enhanced the physical interaction of NR1D1 with PARP1, which is an essential step for the inhibition of DNA repair (24). NR1D1 ligands may induce a conformational change in NR1D1 for the optimal binding to PARP1, particularly under conditions of massive DNA damage. Recently, novel selective ligands for NR1D1, such as GSK2945 and SR12418, with more potent and better pharmacokinetic properties than SR9009, have been identified (42, 45). On the basis of our finding that NR1D1 suppresses breast cancer growth and metastasis, these NR1D1 ligands should be examined for their therapeutic potential against breast cancer, particularly in high NR1D1-expressing tumors.

Figure 6.

NR1D1 activates DNA damage-induced STING signaling in breast cancer cells. **A,** MDA-MB-231 control or *NR1D1* KO cells were treated with 200 μmol/L H_2O_2 for 72 hours or 1 μmol/L doxorubicin for 24 hours. Left, cells were immunostained with anti-γH2AX antibody (green) and nuclei were stained with DAPI (blue). Scale bars, 2 μm. Right, the number of γH2AX foci was quantified in at least 100 cells for each experiment using ImageJ software. The data represent means ± SEM ($n = 3$). Unpaired Student *t* test. **, $P < 0.01$; ***, $P < 0.001$ versus vehicle of each cell type. $^{\#}$, $P < 0.05$ versus control cells; †††, $P < 0.001$ versus control cells treated with H_2O_2 or doxorubicin. **B,** The MDA-MB-231 stable cells were treated with 200 μmol/L H_2O_2 for 72 hours or 1 μmol/L doxorubicin for 24 hours. Left, cells were stained with PicoGreen (green) and Hoechst (blue). Scale bars, 2 μm. Cytosolic DNA intensity was determined by subtracting the intensity of Hoechst staining from that of PicoGreen staining in a cell. Right, staining intensities were quantified in at least 100 cells for each experiment using ImageJ software. The data represent means ± SEM ($n = 3$). Unpaired Student *t* test. *, $P < 0.05$; **, $P < 0.01$; ***, $P < 0.001$ versus vehicle of each cell type; $^{\#}$, $P < 0.05$ versus control cells; ††, $P < 0.01$; †††, $P < 0.001$ versus control cells treated with H_2O_2 or doxorubicin. **C,** The MDA-MB-231 stable cells were treated with 1 μmol/L doxorubicin (Dx) for 24 hours. Left, expression levels of protein were analyzed by Western blotting. Right, band intensities of each phosphorylated protein were quantified using ImageJ and normalized to that of total protein ($n = 3$). Unpaired Student *t* test. *, $P < 0.05$; **, $P < 0.01$; ***, $P < 0.001$ versus vehicle of each cell. $^{\#}$, $P < 0.05$; $^{\#\#}$, $P < 0.01$; $^{\#\#\#}$, $P < 0.001$ versus control cells; ††, $P < 0.01$; †††, $P < 0.001$ versus control cells treated with doxorubicin. **D,** The MDA-MB-231 stable cells were treated with 200 μmol/L H_2O_2 for 72 hours or 1 μmol/L doxorubicin for 24 hours. The amount of IFNα and IFNβ in the cell supernatants was measured by ELISA ($n = 3$). Unpaired Student *t* test. *, $P < 0.05$; **, $P < 0.01$; ***, $P < 0.001$ versus vehicle of each cell type; $^{\#\#\#}$, $P < 0.001$ versus control cells; †††, $P < 0.001$ versus control cells treated with H_2O_2 or doxorubicin.

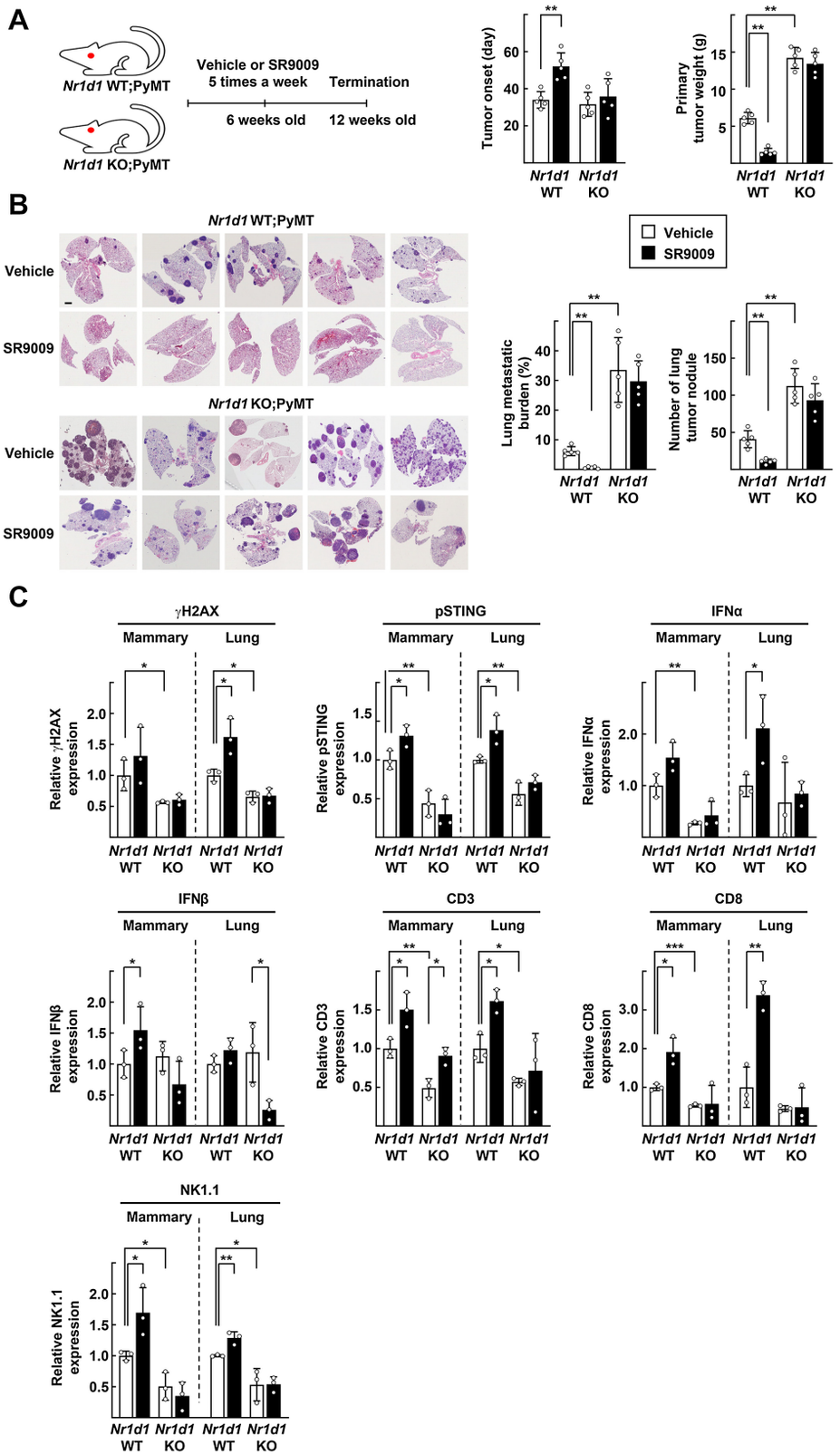

Figure 7.

NR1D1 agonist, SR9009, induces type I IFNs, which inhibits tumor progression and metastasis. **A,** Left, schematic representation of the mouse experiment. Mice were given SR9009 (100 mg/kg/day) or vehicle starting at 6 weeks of age. Right, quantification of time to palpable tumor onset and mammary gland tumor weight from 12-week-old *Nr1d1* WT; PyMT and *Nr1d1* KO;PyMT mice ($n = 5$ per group). Mann–Whitney *U* test. **, $P < 0.01$. **B,** Left, histologic analysis of lung metastasis from 12-week-old *Nr1d1* WT;PyMT and *Nr1d1* KO;PyMT mice. Scale bar, 2 mm. Right, quantification of tumor burden and the number of foci observed in lung tissues from 12-week-old *Nr1d1* WT;PyMT and *Nr1d1* KO;PyMT mice ($n = 5$ per group). Nonparametric Mann–Whitney *U* test. **, $P < 0.01$. **C,** IHC analysis of γH2AX, pSTING, IFNα, IFNβ, CD3, and CD8 in mammary gland and lung tissues from 12-week-old *Nr1d1* WT;PyMT and *Nr1d1* KO;PyMT mice. Staining intensities were quantified from three tumor samples from each group. Representative images are shown in Supplementary Fig. S9. Unpaired Student *t* test. *, $P < 0.05$; **, $P < 0.01$; ***, $P < 0.001$.

Current clinical efforts are focused on developing effective immunotherapy for patients with breast cancer (46). Recently, pembrolizumab, an anti–programmed death 1 mAb, was approved by the FDA for patients with TNBC, expanding treatment options for breast cancer (47). Nevertheless, a large subset of breast cancer represents poor T-cell priming and expansion, which remains the major challenge in breast cancer immunotherapy (48). Thus, recent efforts are being made to develop strategies to enhance immunogenicity and tumor responses to immune checkpoint blockade. Several chemotherapeutic agents, such as taxanes, anthracyclines, and cyclophosphamide, as well as radiotherapy that promotes immunogenic cell death, are currently being investigated in clinical trials in combination with immunotherapy (49). Small molecules, such as STING agonists, toll-like receptor agonists, and indoleamine-2,3-dioxygenase 1 inhibitors, are also being explored as promising combination partners for immune checkpoint blockade (50). In this study, we demonstrated that NR1D1 plays a crucial role in enhancing STING-mediated type I IFN signaling, which leads to the activation and infiltration of $CD8^+$ T cells into tumors and suppresses TANs, TAMs, and Tregs (**Fig. 5**). On the basis of our findings, we suggest that NR1D1 agonists may be good therapeutic candidates to convert immunologically "cold" to "hot" tumors that enhance breast cancer responsiveness to immunotherapy.

Authors' Disclosures

No disclosures were reported.

Authors' Contributions

N.-L. Ka: Conceptualization, formal analysis, funding acquisition, validation, investigation, visualization, writing–original draft, writing–review and editing. **M.K. Park:** Conceptualization, formal analysis, validation, investigation, visualization, writing–original draft, writing–review and editing. **S.-S. Kim:** Data curation, investigation, visualization. **Y. Jeon:** Resources, methodology. **S. Hwang:** Investigation, methodology. **S.M. Kim:** Investigation, methodology. **G.Y. Lim:** Investigation, methodology. **H. Lee:** Conceptualization, supervision, funding acquisition, writing–original draft, project administration, writing–review and editing. **M.-O. Lee:** Conceptualization, supervision, funding acquisition, validation, writing–original draft, project administration, writing–review and editing.

Acknowledgments

This project was supported by grants from the National Research Foundation of Korea (2018R1A5A2024425, 2022R1A2C2006318, and 2022R1C1C2012270), a grant from the National Cancer Center of Korean government (2010271), and Korea Mouse Phenotyping Project (NRF-2014M3A9D5A01073556 and 2014M3A9D5A01075128).

The publication costs of this article were defrayed in part by the payment of publication fees. Therefore, and solely to indicate this fact, this article is hereby marked "advertisement" in accordance with 18 USC section 1734.

Note

Supplementary data for this article are available at Cancer Research Online (http://cancerres.aacrjournals.org/).

Received January 31, 2023; revised May 13, 2023; accepted June 28, 2023; published first July 3, 2023.

References

1. Sung H, Ferlay J, Siegel RL, Laversanne M, Soerjomataram I, Jemal A, et al. Global cancer statistics 2020: GLOBOCAN estimates of incidence and mortality worldwide for 36 cancers in 185 countries. CA Cancer J Clin 2021;71:209–49.
2. Joseph C, Papadaki A, Althobiti M, Alsaleem M, Aleskandarany MA, Rakha EA. Breast cancer intratumour heterogeneity: current status and clinical implications. Histopathology 2018;73:717–31.
3. Gennari A, Conte P, Rosso R, Orlandini C, Bruzzi P. Survival of metastatic breast carcinoma patients over a 20-year period: a retrospective analysis based on individual patient data from six consecutive studies. Cancer 2005;104:1742–50.
4. Dunn GP, Old LJ, Schreiber RD. The three Es of cancer immunoediting. Annu Rev Immunol 2004;22:329–60.
5. Semiglazov V, Tseluiko A, Kudaybergenova A, Artemyeva A, Krivorotko P, Donskih R. Immunology and immunotherapy in breast cancer. Cancer Biol Med 2022;19:609–18.
6. Ali HR, Provenzano E, Dawson SJ, Blows FM, Liu B, Shah M, et al. Association between CD8+ T-cell infiltration and breast cancer survival in 12,439 patients. Ann Oncol 2014;25:1536–43.
7. Salgado R, Denkert C, Campbell C, Savas P, Nuciforo P, Aura C, et al. Tumor-infiltrating lymphocytes and associations with pathological complete response and event-free survival in HER2-positive early-stage breast cancer treated with lapatinib and trastuzumab: a secondary analysis of the neoALTTO trial. JAMA Oncol 2015;1:448–54.
8. Park JH, Jonas SF, Bataillon G, Criscitiello C, Salgado R, Loi S, et al. Prognostic value of tumor-infiltrating lymphocytes in patients with early-stage triple-negative breast cancers (TNBC) who did not receive adjuvant chemotherapy. Ann Oncol 2019;30:1941–9.
9. Asano Y, Kashiwagi S, Goto W, Takada K, Takahashi K, Shibutani M, et al. Predicting therapeutic efficacy of endocrine therapy for stage IV breast cancer by tumor-infiltrating lymphocytes. Mol Clin Oncol 2020;13:195–202.
10. Luen SJ, Salgado R, Fox S, Savas P, Eng-Wong J, Clark E, et al. Tumour-infiltrating lymphocytes in advanced HER2-positive breast cancer treated with pertuzumab or placebo in addition to trastuzumab and docetaxel: a retrospective analysis of the CLEOPATRA study. Lancet Oncol 2017;18:52–62.
11. Yu R, Zhu B, Chen D. Type I interferon-mediated tumor immunity and its role in immunotherapy. Cell Mol Life Sci 2022;79:191.
12. Sokolowska O, Nowis D. STING signaling in cancer cells: important or not? Arch Immunol Ther Exp 2018;66:125–32.
13. Reisländer T, Groelly FJ, Tarsounas M. DNA damage and cancer immunotherapy: a STING in the tale. Mol Cell 2020;80:21–8.
14. Parkes EE, Walker SM, Taggart LE, McCabe N, Knight LA, Wilkinson R, et al. Activation of STING-dependent innate immune signaling by S-phase-specific DNA damage in breast cancer. J Natl Cancer Inst 2017;109:djw199.
15. Ka NL, Lim GY, Hwang S, Kim SS, L MO. IFI16 inhibits DNA repair that potentiates type-I interferon-induced antitumor effects in triple negative breast cancer. Cell Rep 2021;37:110138.
16. Everett LJ, Lazar MA. Nuclear receptor Rev-erbα: up, down, and all around. Trends Endocrinol Metab 2014;25:586–92.
17. Wang S, Li F, Lin Y, Wu B. Targeting REV-ERBα for therapeutic purposes: promises and challenges. Theranostics 2020;10:4168–82.
18. Chin K, DeVries S, Fridlyand J, Spellman PT, Roydasgupta R, Kuo WL, et al. Genomic and transcriptional aberrations linked to breast cancer pathophysiologies. Cancer Cell 2006;10:529–41.
19. Dressman MA, Baras A, Malinowski R, Alvis LB, Kwon I, Walz TM, et al. Gene expression profiling detects gene amplification and differentiates tumor types in breast cancer. Cancer Res 2003;63:2194–9.
20. Kourtidis A, Jain R, Carkner RD, Eifert C, Brosnan MJ, Conklin DS. An RNA interference screen identifies metabolic regulators NR1D1 and PBP as novel survival factors for breast cancer cells with the ERBB2 signature. Cancer Res 2010;70:1783–92.
21. De Mei C, Ercolani L, Parodi C, Veronesi M, Lo Vecchio C, Bottegoni G, et al. Dual inhibition of REV-ERBβ and autophagy as a novel pharmacological approach to induce cytotoxicity in cancer cells. Oncogene 2015;34:2597–608.
22. Wang Y, Kojetin D, Burris TP. Anti-proliferative actions of a synthetic REV-ERBα/β agonist in breast cancer cells. Biochem Pharmacol 2015;96:315–22.
23. Sulli G, Rommel A, Wang X, Kolar MJ, Puca F, Saghatelian A, et al. Pharmacological activation of REV-ERBs is lethal in cancer and oncogene-induced senescence. Nature 2018;553:351–5.
24. Ka NL, Na TY, Na H, Lee MH, Park HS, Hwang S, et al. NR1D1 recruitment to sites of DNA damage inhibits repair and is associated with chemosensitivity of breast cancer. Cancer Res 2017;77:2453–63.

25. Wu J, Hu S, Chen Y, Li Z, Zhang J, Yuan H, et al. BCIP: a gene-centered platform for identifying potential regulatory genes in breast cancer. Sci Rep 2017;7:45235.
26. Terunuma A, Putluri N, Mishra P, Mathé EA, Dorsey TH, Yi M, et al. MYC-driven accumulation of 2-hydroxyglutarate is associated with breast cancer prognosis. J Clin Invest 2014;124:398–412.
27. Győrffy B, Lanczky A, Eklund AC, Denkert C, Budczies J, Li Q, et al. An online survival analysis tool to rapidly assess the effect of 22,277 genes on breast cancer prognosis using microarray data of 1,809 patients. Breast Cancer Res Treat 2010; 123:725–31.
28. Park J, Scherer PE. Adipocyte-derived endotrophin promotes malignant tumor progression. J Clin Invest 2012;122:4243–56.
29. Ka NL, Lim GY, Kim SS, Hwang S, Han J, Lee YH, et al. Type I IFN stimulates IFI16-mediated aromatase expression in adipocytes that promotes E(2)-dependent growth of ER-positive breast cancer. Cell Mol Life Sci 2022;79:306.
30. Na TY, Ka NL, Rhee H, Kyeong D, Kim MH, Seong JK, et al. Interaction of hepatitis B virus X protein with PARP1 results in inhibition of DNA repair in hepatocellular carcinoma. Oncogene 2016;35:5435–45.
31. Na H, Han J, Ka NL, Lee MH, Choi YL, Shin YK, et al. High expression of NR1D1 is associated with good prognosis in triple-negative breast cancer patients treated with chemotherapy. Breast Cancer Res 2019;21:127.
32. Lin EY, Jones JG, Li P, Zhu L, Whitney KD, Muller WJ, et al. Progression to malignancy in the polyoma middle T oncoprotein mouse breast cancer model provides a reliable model for human diseases. Am J Pathol 2003;163:2113–26.
33. Biswas T, Gu X, Yang J, Ellies LG, Sun LZ. Attenuation of TGF-β signaling supports tumor progression of a mesenchymal-like mammary tumor cell line in a syngeneic murine model. Cancer Lett 2014;346:129–38.
34. Kojetin DJ, Burris TP. REV-ERB and ROR nuclear receptors as drug targets. Nat Rev Drug Discov 2014;13:197–216.
35. Shen W, Zhang W, Ye W, Wang H, Zhang Q, Shen J, et al. SR9009 induces a REV-ERB dependent anti-small-cell lung cancer effect through inhibition of autophagy. Theranostics 2020;10:4466–80.
36. Wang H, Fu Y. NR1D1 suppressed the growth of ovarian cancer by abrogating the JAK/STAT3 signaling pathway. BMC Cancer 2021;21:871.
37. Ka NL, Na TY, Lee MO. NR1D1 enhances oxidative DNA damage by inhibiting PARP1 activity. Mol Cell Endocrinol 2017;454:87–92.
38. Wilkenfeld SR, Lin C, Frigo DE. Communication between genomic and non-genomic signaling events coordinate steroid hormone actions. Steroids 2018; 133:2–7.
39. Hammes SR, Davis PJ. Overlapping nongenomic and genomic actions of thyroid hormone and steroids. Best Pract Res Clin Endocrinol Metab 2015; 29:581–93.
40. Khatib T, Marini P, Nunna S, Chisholm DR, Whiting A, Redfern C, et al. Genomic and non-genomic pathways are both crucial for peak induction of neurite outgrowth by retinoids. Cell Commun Signal 2019;17:40.
41. Solt LA, Wang Y, Banerjee S, Hughes T, Kojetin DJ, Lundasen T, et al. Regulation of circadian behaviour and metabolism by synthetic REV-ERB agonists. Nature 2012;485:62–8.
42. Amir M, Chaudhari S, Wang R, Campbell S, Mosure SA, Chopp LB, et al. REV-ERBα regulates T(H)17 cell development and autoimmunity. Cell Rep 2018;25: 3733–49.
43. Meng QJ, McMaster A, Beesley S, Lu WQ, Gibbs J, Parks D, et al. Ligand modulation of REV-ERBalpha function resets the peripheral circadian clock in a phasic manner. J Cell Sci 2008;121:3629–35.
44. Dierickx P, Emmett MJ, Jiang C, Uehara K, Liu M, Adlanmerini M, et al. SR9009 has REV-ERB-independent effects on cell proliferation and metabolism. Proc Natl Acad Sci U S A 2019;116:12147–52.
45. Trump RP, Bresciani S, Cooper AW, Tellam JP, Wojno J, Blaikley J, et al. Optimized chemical probes for REV-ERBα. J Med Chem 2013;56:4729–37.
46. Pellegrino B, Tommasi C, Cursio OE, Musolino A, Migliori E, De Silva P, et al. A review of immune checkpoint blockade in breast cancer. Semin Oncol 2021;48: 208–25.
47. Schmid P, Cortes J, Pusztai L, McArthur H, Kümmel S, Bergh J, et al. Pembrolizumab for early triple-negative breast cancer. N Engl J Med 2020; 382:810–21.
48. Henriques B, Mendes F, Martins D. Immunotherapy in breast cancer: when, how, and what challenges? Biomedicines 2021;9:1687.
49. Meric-Bernstam F, Larkin J, Tabernero J, Bonini C. Enhancing anti-tumour efficacy with immunotherapy combinations. Lancet 2021;397:1010–22.
50. Zhu HF, Li Y. Small-molecule targets in tumor immunotherapy. Nat Prod Bioprospect 2018;8:297–301.